

Nucleon-anti-nucleon intruder state of Dirac equation for nucleon in deep scalar potential well

T.T.S. Kuo^{a1}, T.K. Kuo^b, E. Osnes^c, S. Shu^{a,d}

^a*Department of Physics and Astronomy, Stony Brook University,
Stony Brook, NY 11794, USA*

^b*Physics Department, Purdue University, W. Lafayette, IN 47907, USA*

^c*Institute of Physics, University of Oslo, NO 0316 Oslo, Norway*

^d*Department of Physics and Electronic Science, Hubei Univ.,
Wuhan 430062, China*

We solve the Dirac radial equation for a nucleon in a scalar Woods-Saxon potential well of depth V_0 and radius r_0 . A sequence of values for the depth and radius are considered. For shallow potentials with $-1000\text{MeV} \lesssim V_0 < 0$ the wave functions for the positive-energy states $\Psi_+(r)$ are dominated by their nucleon component $g(r)$. But for deeper potentials with $V_0 \lesssim -1500\text{MeV}$ the $\Psi_+(r)$ s begin to have dominant anti-nucleon component $f(r)$. In particular, a special intruder state enters with wave function $\Psi_{1/2}(r)$ and energy $E_{1/2}$. We have considered several r_0 values between 2 and 8 fm. For $V_0 \lesssim -2000\text{MeV}$ and the above r_0 values, $\Psi_{1/2}$ is the only bound positive-energy state and has its $g(r)$ closely equal to $-f(r)$, both having a narrow wave-packet shape centered around r_0 . The $E_{1/2}$ of this state is practically independent of V_0 for the above V_0 range and obeys closely the relation $E_{1/2} = \frac{\hbar c}{r_0}$.

1. Introduction

Intruder states have played an important role in nuclear structure physics. Two of us (TTSK and EO) first learned of this subject from Gerry Brown when we were his postdocs at respectively Princeton and Nordita some long time ago. Gerry has taught, inspired and helped both of us a great deal; we are deeply grateful to him and remember well the pleasant time we had with him.

The nuclear shell model is a most successful model for nuclear structure. A desirable feature is its large energy gap between major shells. For example, the large energy gap between the $1s0d$ and $0p$ shells allows us to treat the nucleus ^{18}O using a small $2p0h$ model space, namely treating it

¹thomas.kuo@stonybrook.edu

simply as two $0s1d$ valence nucleons outside a closed ^{16}O core. Pioneered by Gerry, a large number of shell-model studies of nuclei using realistic nucleon-nucleon interactions have been carried out.¹⁻⁸ The importance of intruder states in model-space effective interactions has been investigated by Schucan and Weidenmueller and others.^{9,10}

In Fig.1 we display the results of a typical calculation of ^{18}O .⁷ In this calculation, a low-momentum interaction V_{lowk} is employed, and the shell-model effective interaction has been calculated using three effective interaction methods denoted by LS, KK and EKKO⁷ in the figure. As seen, calculations give only two 2^+ states while experiments have three. The missing one is an 'intruder' state whose wave function is mainly outside the $2p0h$ space which is the model space used for such calculation. The energies of the unperturbed $4p2h$ states are much higher than the $2p0h$ ones. But when the interaction is strong, some $4p2h$ states are pushed down, forming an intruder 2^+ state whose energy is as low as those states which are dominated by the $2p0h$ components. The presence of the intruder state is an indication that the Fermi sea (^{16}O -core) is no longer closed when the interaction is strong.

In the present short contribution dedicated to the memory of Gerry, we shall study the Dirac equation for a nucleon in a strong scalar potential well and discuss its possible intruder states. For a free nucleon, the negative-energy Dirac sea is closed. But when it is subject to a strong external field, it may be no longer closed and in analogy to the nuclear case described above, give rise to nucleon-anti-nucleon intruder states.

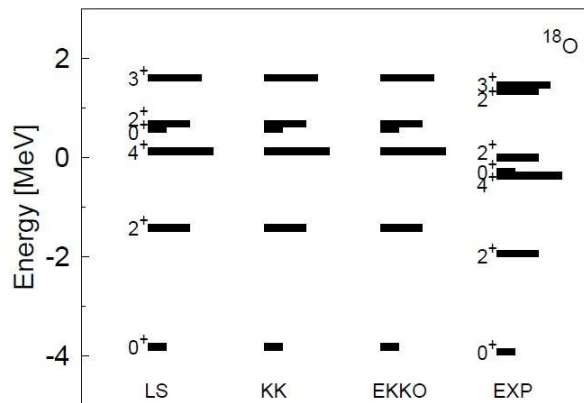


Fig. 1. Intruder states in low energy spectrum of ^{18}O

Before discussing our present work, we would like to mention briefly Gerry's style of physics; he was fond of and successful in using simple models to bring out the simple physics of complicated problems. He often said 'This is too complicated; I can not check it with my 5-dollar calculator'. The Brown-Bolsterli schematic model for nuclear giant dipole resonance is a well known example.¹¹ The second-order core polarization diagram for nuclear effective interaction is another example, and has played an essential role in microscopic nuclear structure studies.¹⁻⁸ How would the properties of hadrons change with their surrounding medium is a quite complicated problem. But the Brown-Rho scaling^{12,13} provides a remarkably simple answer, namely $m^*/m = 1 - Cn/n_0$ where m^* and m are respectively the in-medium and in-vacuum hadron mass. The medium density is n and the nuclear matter saturation density n_0 . For low densities, $C \simeq 0.2$. Extensive applications of the Brown-Rho scaling on nuclear matter, neutron stars and the long life-time β -decay of ^{14}C have been carried out.¹⁴⁻²⁰

In the following we shall first describe some details for solving the Dirac radial equation with a scalar central potential V_s (section 2). To mimic the extremely strong potential which may be present in highly compacted stellar objects, we shall consider the Dirac equation for a nucleon in super-deep scalar potentials in section 3. The resulting nucleon-anti-nucleon intruder states will be discussed. In the final section 4 we present a summary and conclusion.

In order to elucidate our calculation by a simple pedagogical example, we have repeated the calculation using a one-dimensional Woods-Saxon potential; this is included in an Appendix.

2. Dirac radial equation with scalar potential well

We consider the Dirac equation for a nucleon

$$[c(\boldsymbol{\alpha} \cdot \mathbf{p}) + \beta(mc^2 + V_s) + V_v]\psi = E\psi \quad (1)$$

where m denotes its mass, and V_s and V_v respectively the scalar and vector potential. Its radial equation²²⁻²⁴ is

$$\begin{aligned} \frac{dg(r)}{dr} &= -\frac{k}{r}g(r) + \frac{1}{\hbar c}[E - V_v(r) + V_s(r) + mc^2]f(r) \\ \frac{df(r)}{dr} &= +\frac{k}{r}f(r) - \frac{1}{\hbar c}[E - V_v(r) - V_s(r) - mc^2]g(r) \end{aligned} \quad (2)$$

with

$$k = \begin{cases} -(l+1), & j = l + 1/2 \\ l, & j = l - 1/2 \end{cases} \quad (3)$$

and

$$\psi_{jlm} = \frac{1}{r} \begin{bmatrix} ig(r)y_{lm}^j \\ -f(r)y_{l'm}^j \end{bmatrix} \quad (4)$$

where $l' = 2j - l$. In the above, we use $mc^2=938$ MeV and $\hbar c=197.3$ MeV-fm. We shall consider in the present work the $l = 0$ and $j = 1/2$ state (namely $k=-1$).

To determine the bound-state eigenvalues of the above Dirac radial equations, a standard procedure is to integrate from $r=0$ to r_{end} in two portions: (I) from $r = 0$ to r_{match} obtaining wave functions g_I and f_I , and (II) from r_{end} to r_{match} obtaining g_{II} and f_{II} , where $0 < r_{match} < r_{end}$. For an energy variable ω equal to a bound-state eigenvalue the logarithmic boundary conditions at r_{match} are satisfied, namely

$$\frac{d}{dr} \log(g_I(\omega, r_{match})) = \frac{d}{dr} \log(g_{II}(\omega, r_{match})), \quad \omega = E_1, E_2, \dots, \quad (5)$$

and

$$\frac{d}{dr} \log(f_I(\omega, r_{match})) = \frac{d}{dr} \log(f_{II}(\omega, r_{match})), \quad \omega = E_1, E_2, \dots. \quad (6)$$

Note that the above two conditions are theoretically equivalent, but 'numerically' they are often not. High accuracy is generally needed for calculating the above quantities, and when this is not met they may give different and spurious eigenvalues.

In the present work we employ the following alternative matching condition for determining the eigenvalues, namely

$$\frac{f_I(\omega, r_{match})}{g_I(\omega, r_{match})} = \frac{f_{II}(\omega, r_{match})}{g_{II}(\omega, r_{match})}. \quad (7)$$

This single condition is 'theoretically' equivalent to the previous two conditions, Eqs.(5) and (6). But 'numerically' we have found it being considerably more accurate and efficient. In our calculations, we shall mainly use this matching condition. We shall also use both Eqs.(5) and (6) and a visual inspection of the resulting wave functions to double check our results.

We consider a nucleon in a scalar Woods-Saxon potential well

$$V_s(r) = \frac{V_0}{1 + e^{(r-r_0)/\delta}} \quad (8)$$

with well depth V_0 . We shall use a range of V_0 values from about -50 to minus few-thousand MeV. (Possible connection of our choices with dense stellar objects like black holes will be discussed in section 4.) We shall also consider a range of r_0 values. For convenience we shall use $\delta=0.1$ fm for

all calculations. The values for r_{match} and r_{end} are dependent on r_0 . For example for $r_0 = 4$ fm we use $r_{end} = 6$ fm and $r_{match} = 4.5$ fm. For this case we have also used $r_{match} = 5.0$ fm, with results in very good agreement (to 4th decimal place) with the former.

To illustrate our calculations, we first present some of our results with a $V_0 = -50$ MeV potential, $r_0 = 4$ fm and δ as given above. As seen in Fig. 2, the wave function of E_{1+} is largely dominated by its nucleon component $g(r)/r$. But the wave function for the negative energy E_{1-} is dominated by its anti-nucleon component $f(r)/r$ as seen in Fig. 3. In Fig. 4 we consider the wave functions corresponding of the E_{2+} state of the same potential. They are still dominated by $g(r)/r$ but have a slightly larger $f(r)/r$ component than E_{1+} . Note both of the wave functions in Fig. 4 have a node. Our scheme for ordering the positive energy states is $E_{1+} < E_{2+} < E_{3+} < \dots$ and $\dots < E_{3-} < E_{2-} < E_{1-}$ for the negative energy ones.

These wave functions and those to be displayed later are normalized without the angular integration factor 4π , namely

$$\int (f(r)^2 + g(r)^2) dr = 1. \quad (9)$$

The above optical potential is similar to the empirical optical potentials used for a nucleon in a nucleus of mass number $A \simeq 40$.^{21,22} Our results indicate that for such ordinary nuclear systems the positive energy states of their nucleons are dominated by their nucleon component $g(r)$.

3. Nucleon anti-nucleon level crossing and intruder state

In Table 1, we present our results for a Dirac nucleon in the above potential well with different well depths V_0 . Before discussing our results, let us mention that the matching conditions addressed earlier depends very sensitively on the energy variable ω . Thus, a very small change in ω can drastically change the wave functions f and g . As shown in Table 1, we have determined the energies E very accurately so as to satisfy the matching conditions. It is our hope that interested readers may check our numerical results.

Let us now discuss the results listed in Table 1. In Fig. 5 we plot the energies of of the $1-$, $1+$ and $2+$ states versus V_0 . As seen there is clearly a level-crossing behavior; the nucleon level E_{1+} descends with V_0 whereas the anti-nucleon E_{1-} level ascends. They 'cross' at a crossing potential of $V_0 \simeq -1000 \text{ MeV} \simeq -mc^2$. (In fact they can not actually cross for real

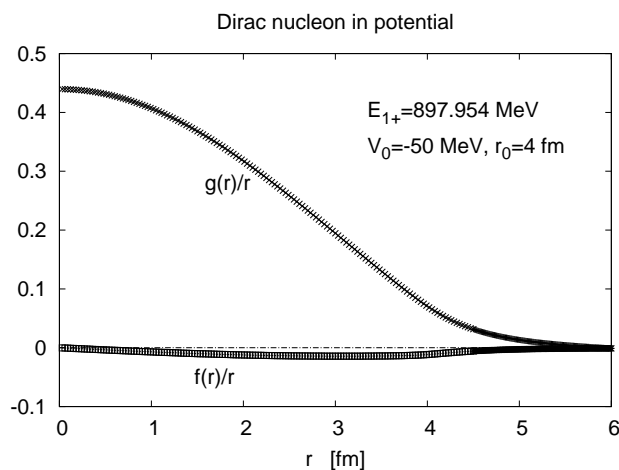


Fig. 2. Dirac wave functions for $E_{1+}=897.952 \text{ MeV}$ and $V_0=-50 \text{ MeV}$.

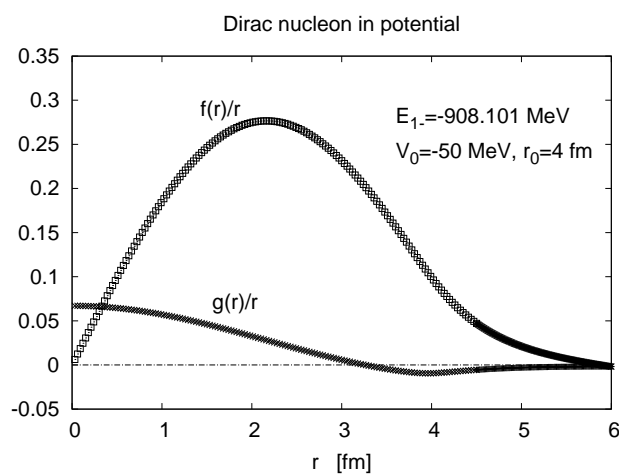


Fig. 3. Same as Fig. 2 but for $E_{1-}=-908.100 \text{ MeV}$.

V_0 , but can do so for complex V_0 .⁹) In Fig.6, we plot the corresponding anti-nucleon fractions $\langle f|f \rangle$. As the well becomes deeper, the anti-nucleon fraction of the $1-$ state drops monotonically from ~ 1 at shallow well to ~ 0 at deep well of $V_0 \simeq -2000 \text{ MeV}$. In other words, this anti-nucleon is 'transmuted' into a nucleon in the process. We note that the crossing

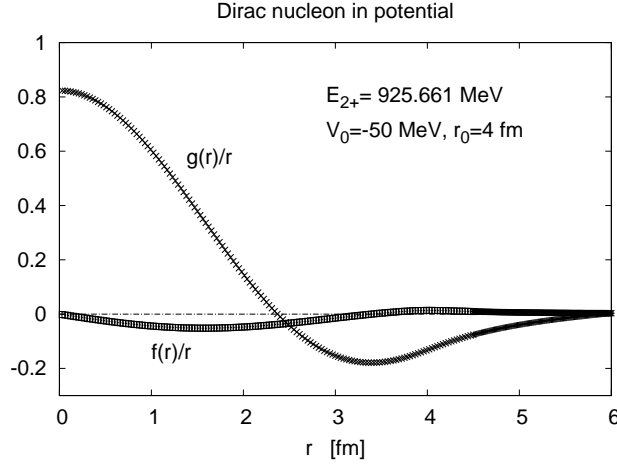


Fig. 4. Same as Fig. 2 but for $E_{2+}=925.661$ MeV.

Table 1. Energies and anti-nucleon fraction $\langle f|f \rangle$ of a nucleon in scalar Woods-Saxon potentials of depth V_0 . The widths of these potentials are all $r_0=4$ fm. The subscripts 1+ and 1- refer to respectively the lowest positive- and highest negative-energy state. V_0 and E are both in units of MeV.

V_0	E_{1-}	$\langle f f \rangle_{1-}$	E_{1+}	$\langle f f \rangle_{1+}$
-50	-908.101	0.9908	897.954	0.004645
-100	-861.325	0.9883	849.499	0.005851
-300	-671.036	0.9780	654.283	0.01098
-500	-485.047	0.9570	461.309	0.02180
-700	-313.559	0.8594	275.994	0.05498
-900	-194.461	0.6487	120.856	0.2011
-1000	-191.321	0.3894	76.8122	0.3537
-1100	-236.603	0.1854	59.8212	0.4574
-1300	-397.210	0.05180	52.5618	0.4917
-1500	-583.955	0.02299	50.7829	0.4960
-1700	-777.233	0.01515	49.9197	0.4973

potentials for E and $\langle f|f \rangle$ are approximately the same.

We now consider the evolution of the energy and anti-nucleon fraction of the 1+ state in Figs. 5 and 6. As the well becomes deeper, its energy drops till about $V_0 \simeq -1000$ MeV. And until this strength is reached, this anti-nucleon fraction keeps on rising. But afterwards a plateau of energy

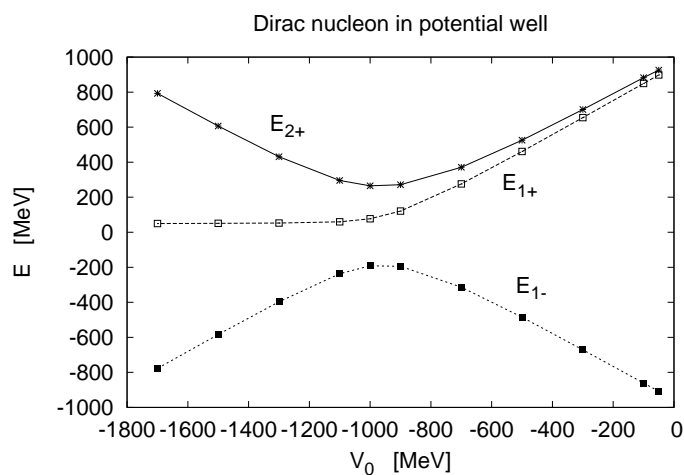


Fig. 5. Energy levels of nucleon in potential wells of different well depths V_0 .

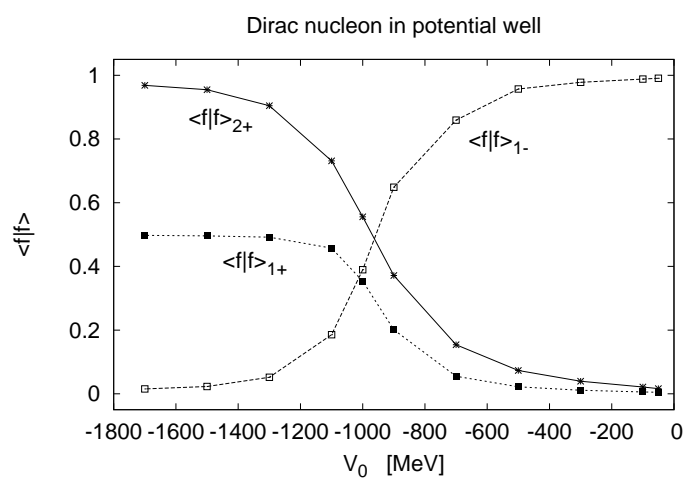


Fig. 6. Anti-nucleon fractions of nucleon in potential wells of different well depths V_0 .

$\simeq 50$ MeV and $\langle f|f \rangle \simeq 0.50$ is reached. It is of interest that this nucleon is approaching some sort of 'hybrid nucleon' composed of half nucleon and half anti-nucleon. It may be noted that, as indicated by Fig. 5, this hybrid state is the only bound state for $V_0 < \sim -2000$ MeV, while all other states

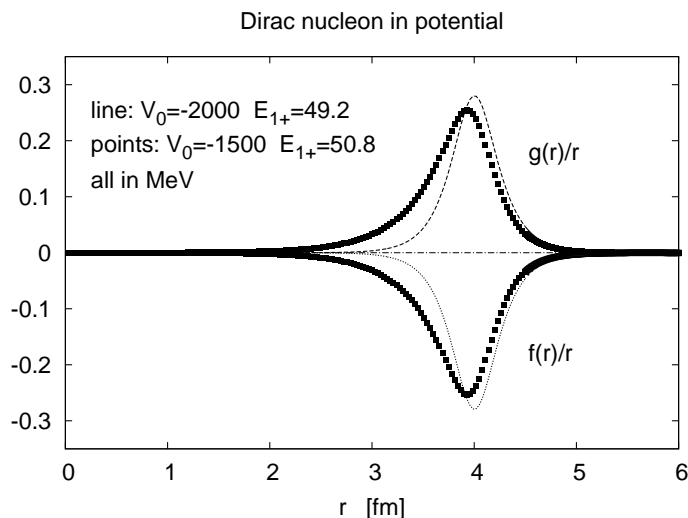


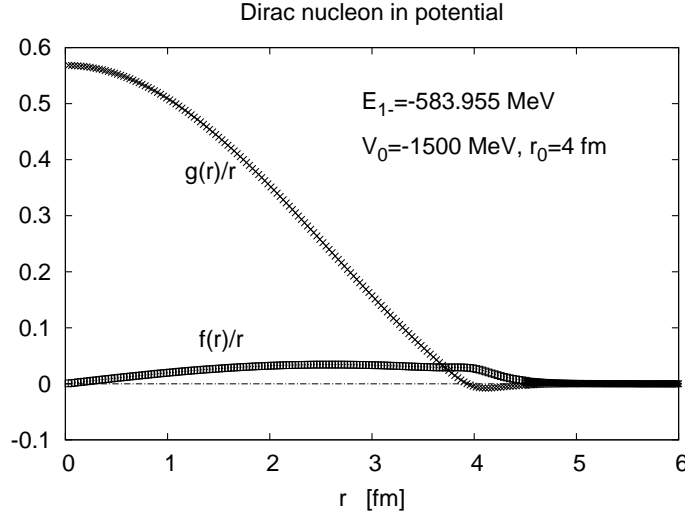
Fig. 7. Wave functions of a Dirac nucleon in a super-deep potential well of depth $V_0 = -1500$ MeV with energy $E_{1+} = 50.7829$ MeV. Those of the corresponding state for $V_0 = -2000$ MeV are also shown.

are diverging outward having energies $|E| > mc^2$. (By bound state we mean a state of energy being $|E| < mc^2$.)

In Fig. 7 we display the wave function of such a hybrid nucleon belonging to the $V_0 = -1500$ MeV potential. It is amusing that the radial distributions of its nucleon and anti-nucleon components are almost identical, except for a sign change in the wave function. Furthermore, this hybrid nucleon has the mass largely concentrated near its surface, making it a hollow nucleon. In this figure, the corresponding wave function for $V_0 = -2000$ MeV is also shown. It has a similar Gaussian wave packet shape, but of narrower width.

The wave function of the $1-$ anti-nucleon belonging to the same -1500 MeV potential is displayed in Fig. 8. As seen, it has almost no anti-nucleon content; it is a 'nucleon' evolved from its parent anti-nucleon. The wave function of the $2+$ state of this potential is shown in Fig. 9. Its $f(r)$ component is much larger than the $g(r)$ one, indicating this positive energy nucleon is actually predominantly composed of anti-nucleon.

Let us now discuss the results from potentials deeper than those shown in Table 1. In Fig. 10 we focus on the $1+$ state calculated with different well depths. Plotted are the anti-nucleon fraction $\langle f|f \rangle$ and the effective

Fig. 8. Same as Fig.7 but for energy $E_{1-} = -583.955$ MeV.

mass defined as $m^*/m \equiv E_{1+}/(mc^2)$ where m is the free nucleon mass. Near zero potential, we have $m^*/m \simeq 1$ and $\langle f|f \rangle \simeq 0$. As V_0 becomes more negative, the former descends and the latter ascends until $V_0 \simeq -1500$ MeV. Afterwards, its m^*/m remains flat at about 0.05 (corresponding to $E_{1+} \simeq 50$ MeV) and its $\langle f|f \rangle$ is flat at about 0.50. In the figure we show results down to $V_0 \simeq -3500$ MeV. We have tried deeper potentials, in fact as deep as $V_0 = -5400$ MeV, and the flatness of these two curves remains unchanged. It seems that the above E_{1+} and $\langle f|f \rangle_{1+}$ are practically independent of V_0 for $V_0 < \sim -1500$ MeV. The wave function and energy of this 'flat' state will be referred to as $\Phi_{1/2}$ and $E_{1/2}$ respectively.

Our results presented above are all obtained numerically. It would be nice if they can be obtained analytically. We have tried but so far have not succeeded. To partially understand the above 'flatness' behavior of Figs. 5, 6 and 10, let us rewrite Eq.(2) in matrix form as

$$\begin{bmatrix} -(V_s + mc^2)/\hbar c & \frac{d}{dr} + \frac{k}{r} \\ -\frac{d}{dr} + \frac{k}{r} & (V_s + mc^2)/\hbar c \end{bmatrix} \begin{bmatrix} f \\ g \end{bmatrix} = E \begin{bmatrix} f \\ g \end{bmatrix}. \quad (10)$$

Here we do not have the V_v term of Eq.(2) as we include only the scalar potential V_s .

The diagonal terms $-(V_s + mc^2)$ and $(V_s + mc^2)$ play an important role in the above equation. When $V_s \simeq 0$, the wave functions of the positive-

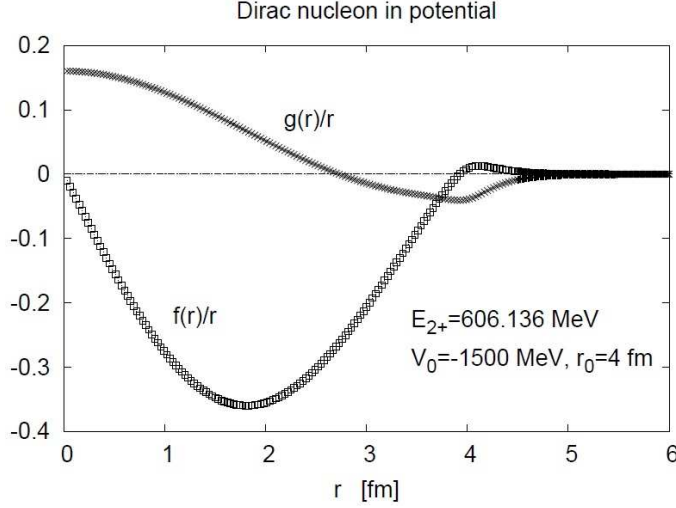


Fig. 9. Same as Fig.7 but for energy $E_{2+}=606.136$ MeV.

and negative-energy states are dominated by their nucleon and anti-nucleon component $g(r)$ and $f(r)$ respectively. But when V_s is largely negative, say -2000 MeV, $\langle f | -(V_s + mc^2) | f \rangle$ becomes positive while $\langle g | (V_s + mc^2) | g \rangle$ becomes negative. Then the positive-energy state is dominated by the anti-nucleon component $f(r)$ while the negative-energy one by $g(r)$. This explains the level crossing seen in Fig. 5 for the $1-$ to $2+$ right-to-left cross over and similarly the $2+$ to $1-$ cross over.

The middle $1+$ state of Fig. 5 is, however, a special case. Its energy E_{1+} for $V_0 < \sim -1500$ MeV is not only nearly independent of V_0 but is also rather small (~ 50 MeV). These properties suggest that there must be some cancellation among the contributions from V_s to this state, leading to a near-zero net contribution. A possible way to attain such cancellation is to have either $f = -g$ or $f = g$ where f and g are respectively the anti-nucleon and nucleon component of the eigenfunction of this $1+$ state.

To study this possible cancellation, we rewrite Eq.(10) as

$$[-(V_s + mc^2)/(\hbar c) + \frac{d}{dr}](f + g) - \frac{k}{r}(f - g) = E(f - g) \quad (11)$$

and

$$[-(V_s + mc^2)/(\hbar c) - \frac{d}{dr}](f - g) + \frac{k}{r}(f + g) = E(f + g). \quad (12)$$

We have used the above equations to calculate the wave functions $(f+g)$ and $(f-g)$. These calculations can also be performed equivalently using

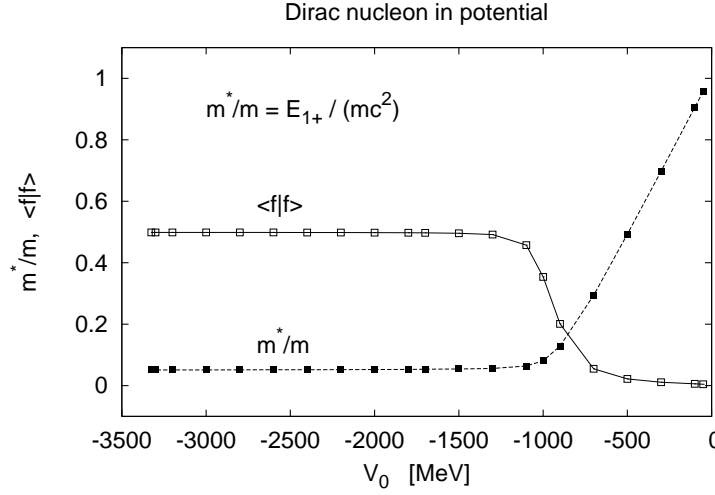


Fig. 10. Evolution of the E_{1+} energies and their anti-nucleon fractions with potential depth V_0 . A potential radius of $r_0=4$ fm is used for all calculations shown.

Eq.(10). We have found for $V_0 \lesssim -1400$ MeV ($1.5mc^2 = 1407$ MeV), the wave function (f+g) is very much smaller than (f-g) for the 1+ state. We have calculated for this state the norm $N_+ \equiv \langle f + g | f + g \rangle$ and $N_- \equiv \langle f - g | f - g \rangle$ with the normalization $N_+ + N_- = 1$. Our results are $(N_+, N_-) = (0.00004, 0.99996)$ for $V_0 = -1400$ MeV and $(0.00002, 0.99998)$ for $V_0 = -1500$ MeV. In both calculations $r_0 = 4$ fm is used.

Thus for the 1+ state with $V_0 \lesssim -1500$ MeV, we can drop the (f + g) terms relative to the (f - g) ones in the above equations. Then Eq. (11) gives the simple energy relation

$$E = -k\hbar c \frac{\langle g|1/r|g \rangle}{\langle g|g \rangle} \quad (13)$$

for the energy of the 1+ state. Recall that $k = -1$ (see section 2). To calculate the above energy, we need to have $\langle g|1/r|g \rangle$.

If $\langle g|1/r|g \rangle / \langle g|g \rangle$ is independent of V_0 , then so is the above energy. In fact we have found that for $V_0 \lesssim -1500$ MeV, $(\langle g|1/r|g \rangle / \langle g|g \rangle)$ is closely equal to $1/r_0$ and is nearly independent of V_0 . Thus the above energy is only weakly dependent on V_0 as indicated by Fig. 10 and Table 1. For the above V_0 range, g is generally of a Gaussian wave packet shape narrowly peaked around r_0 . In Fig. 7 we have displayed such wave functions for $r_0 = 4$ fm. We have found that the wave functions for other

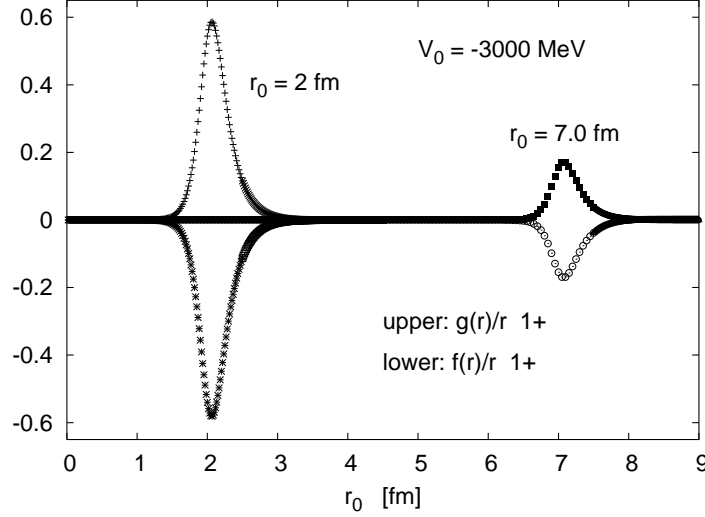


Fig. 11. Radial wave functions $g(r)/r$ and $f(r)/r$ for the $1+$ state of potential wells $V_0 = -3000$ MeV and $r_0 = 2$ and 7 fm.

choices of r_0 are also of this shape. In Fig. 11 we display two such wave functions for $r_0 = 2$ and 7 fm. This special shape of the wave functions renders $\langle g|1/r|g \rangle / \langle g|g \rangle \simeq 1/r_0$ a good approximation. With this approximation, Eq. (13) becomes then

$$E \simeq \frac{-k\hbar c}{r_0}. \quad (14)$$

The accuracy of this approximation will be discussed later.

We have considered Eq. (11) for $f \simeq -g$. Let us now consider Eq. (12). In this situation we can drop the $(f+g)$ terms there and have

$$\frac{dg}{dr} = -g(V_s + mc^2)/(\hbar c) \quad (15)$$

which is a simple differential equation for determining the wave function g . For the Woods-Saxon potential of Eq.(8), the above equation gives

$$g(r) = \exp\left[-\frac{V_0}{\hbar c}[(r - r_0) - \delta \log(1 + e^{(r-r_0)/\delta})] - \frac{mc^2}{\hbar c}r\right]. \quad (16)$$

Note that the above expression does not include the normalization constant. For $V_0 \lesssim -1500$ MeV the wave function calculated with the above equation agrees very well with the corresponding result from solving the full Dirac equation of Eq. (10).

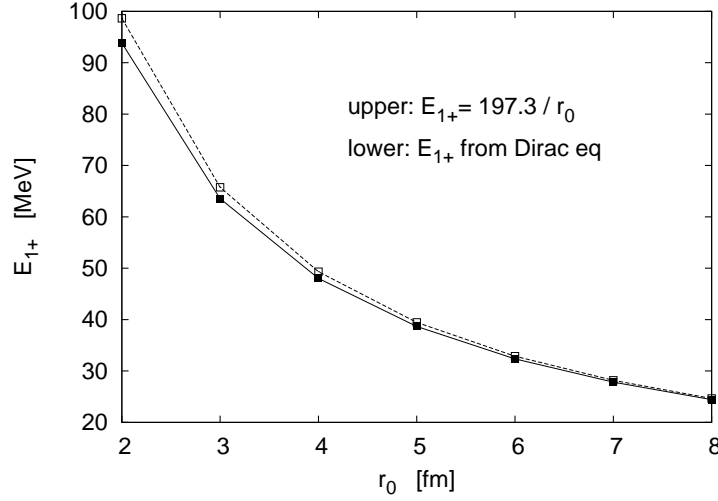


Fig. 12. Dependence of the 1+ energy on the range r_0 of the WS potential well. Common well depth of $V_0 = -3000$ MeV is used.

The following approximation is helpful in understanding the structure of the $g(r)$ wave function. For r close to r_0 , the Woods-Saxon potential of Eq.(8) can be approximated by a linear potential, namely

$$V_s(r) \rightarrow \frac{V_0}{2} \left[1 - \frac{r - r_0}{2\mu} \right]. \quad (17)$$

Then Eq.(15) gives

$$g(r) \propto \exp\left[\frac{V_0}{8\mu}(r - r_0)^2\right] \quad (18)$$

which is of Gaussian form, providing an explanation for the shape of the wave functions displayed in Figs. 7 and 11.

The parameter μ of Eq.(17) is determined by fitting the WS potential near r_0 . As an example, we find $\mu = 0.144$ by fitting the $r_0 = 4$ fm and $V_0 = -2000$ MeV potential in the range of $r = 3.7$ to 4.3 fm. Then the wave function given by Eq.(18) is of the form $\exp[b(r - r_0)^2]$ with $b = V_0/(\hbar c 8\mu) = -8.80$. The same wave function obtained by solving the Dirac equations of Eq. (10) has been given in Fig. 7. Fitting it by $\alpha \cdot \exp[\beta(r - \gamma r_0)^2]$ gives $\alpha = 1.07$, $\beta = -8.37$ and $\gamma = 1.004$. Note that the β value is close to the above b value.

To estimate the accuracy of the energy approximation of Eq.(14), we have compared the energies so obtained with those from the full calculation

of Eq. (10). Some sample comparisons are given in Fig. 12 where the energies for the $1+$ state calculated from Eq.(10) using $V_0 = -3000$ MeV and $r_0 = 2$ to 7 fm are compared with those given by Eq.(14). It is of interest that the two sets of energies agree remarkably well, indicating this approximation being highly accurate. Note that Eq. (14) is independent of V_0 . This is consistent with Fig. 10 where the energies of the $1+$ state are nearly independent of V_0 for $V_0 \lesssim -1500$ MeV.

For particles of zero rest mass, the momentum-position uncertainty principle may be written as $\Delta E \Delta r \simeq \hbar c$; $E = pc$. It is of interest that the energy relation of this special state as given by Eq. (14) is similar to this uncertainty principle, suggesting that the nucleon in this special state has a near-vanishing effective mass as indicated by Fig. 10.

4. Summary and discussion

In the present work we have solved the Dirac radial equation for a nucleon in a scalar Woods-Saxon potential well with depth V_0 and radius r_0 . For weak potentials such as $V_0 \simeq -50$ MeV, the positive-energy states Ψ_+ of this equation have energies $\simeq +mc^2$ and wave functions dominated by the nucleon component $g(r)$, as indicated by Figs. 2 and 6. Similarly the negative-energy states Ψ_- have energies close to $-mc^2$ and wave functions dominated by the anti-nucleon component $f(r)$ as illustrated in Fig. 3.

As V_0 turns more negative (deeper), a qualitative reversal of the wave functions takes place. Namely, Ψ_- is generally becoming increasingly dominated by $g(r)$, and so is Ψ_+ by $f(r)$. Examples illustrating such tendencies are displayed in Figs. 8 and 9.

The lowest positive-energy state 1_+ is however an exemption, being a special intruder state. As indicated by Figs. 5 and 6, at weak potential strength this state has $E_{1_+} \simeq mc^2$ and $\langle f | \Psi_{1_+} \rangle^2 \simeq 0$. But as V_0 becomes $\lesssim -1500$ MeV, this state is characterized by a special wave function $\Psi_{1/2}$ with constant composition of $f = -g$ where g and f are respectively its nucleon and anti-nucleon component and both are narrowly peaked around r_0 . In addition, the energy of this state approaches a constant energy $E_{1/2} \simeq \hbar c/r_0$. These behaviors have been illustrated in Figs. 5, 6 and 10. For $V_0 \lesssim -2000$ MeV, our results suggest that the above state, with wave function $\Psi_{1/2}$ and energy $E_{1/2}$, is the only bound state. It should be of interest if one could check this special intruder state experimentally. We note that a hypothetical scalar Woods-Saxon potential of very strong strength has been used in our work for calculating this and other intruder

states. Is such a strong potential conceivable?

We have estimated that a nucleon near the surface of a medium-mass black hole (of mass $\sim 10^3$ solar mass and radius $\sim 10^3$ km^{25,26}) would experience a gravitational potential of approximately -1400 MeV ($\cong 1.5mc^2$). There has been evidence for super-massive black holes such as the 4.3×10^6 solar-mass black hole in the Milky Way.^{25,26} They may produce similar or stronger gravitational potential. Thus, the special nucleons indicated by this work may be present near such black holes.⁹ This needs of course further study. With the presence of such strong gravitational field we may need to use a Dirac equation in curved spacetime.^{28,29} whereas we have been using the Dirac equation in flat spacetime. It would indeed be of interest to obtain an estimate of the effects introduced by curved spacetime.

Let us end by quoting a paragraph written by Gerry:⁶

“One of the authors, Gerry Brown, arrived at Princeton in early September, 1964. The next morning, as he came to the Palmer Physics Laboratory, Eugene Wigner, who just preceded him, opened the door for him (It was a real contest to get ahead of Eugene and open the door for him which very few succeeded in doing.) Eugene asked Gerry, as we went into the building, what he planned to work on. ‘I plan to work out the nucleon-nucleon interaction in nuclei.’ Eugene said that it would take someone cleverer than him, to which Gerry replied that they probably disagreed what it meant to ‘work out’. Gerry wanted to achieve a working knowledge, sufficiently good to be able to work out problems in nuclear physics.”

In fact, it is our hope that the present calculations may serve as a warm-up exercise for ‘working out’ the Dirac equation for nucleons experiencing extremely strong scalar potential fields and its possible connection with dense stellar objects.

Acknowledgement: We thank Edward Shuryak, Ismail Zahed and Jeremy Holt for many helpful discussions. This work is supported by the US Department of Energy under contract DE-FG02-88ER4038. S. Shu is supported by the China Scholarship Council.

Appendix: In this Appendix the nucleon-anti-nucleon intruder states mentioned earlier are studied using a simpler and more transparent model. As indicated by Eq.(5), our earlier calculations are based on a model where a nucleon is placed in a spherical Woods-Saxon (WS) potential. When the depth of this potential is deeper than a certain value, the ground state of

⁹We have also made a similar estimate for a neutron star of mass $2.1M_{\odot}$ ²⁷ and radius ~ 11 km.²⁰ The resulting potential is about -270 MeV. Thus we do not expect the presence of such special nucleons near this neutron star, as indicated by Fig.10.

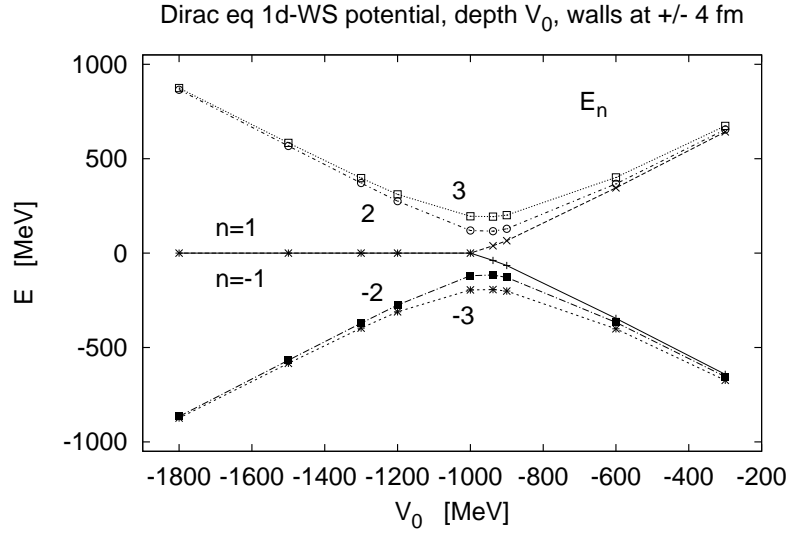


Fig. 13. Energies of Dirac equation for a nucleon in a one-dimensional scalar WS potential. A similar plot for the spherical WS potential used earlier is shown in Fig. 3.

the nucleon becomes a special half-nucleon intruder state. One might ask if this holds true also for a one-dimensional Woods-Saxon potential.

To answer this question, we have repeated our earlier calculations using a one-dimensional WS potential

$$V_s(x) = V_0 \left[1 + \exp\left(\frac{xS(x) - x_0}{\delta}\right) \right]^{-1}; \quad S(x) = x/|x|. \quad (19)$$

The corresponding Dirac equation is

$$\begin{bmatrix} A & B \\ -B & -A \end{bmatrix} \begin{bmatrix} f \\ g \end{bmatrix} = E \begin{bmatrix} f \\ g \end{bmatrix} \quad (20)$$

with

$$A = -(V_s(x) + mc^2)/(\hbar c), \quad B = \frac{d}{dx}. \quad (21)$$

The solutions of this equation are paired, namely

$$E_{n+} = -E_{n-}; \quad (f_{n+}, g_{n+}) = \pm(g_{n-}, f_{n-}) \quad (22)$$

for all n. Eq.(20) can be rewritten as

$$\begin{aligned} (A - B)(A + B)(f + g) &= E^2(f + g) \\ (A + B)(A - B)(f - g) &= E^2(f - g). \end{aligned} \quad (23)$$

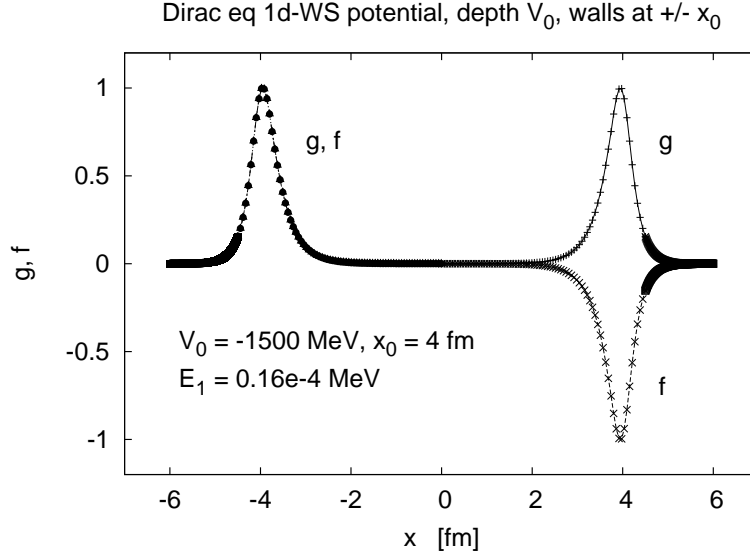


Fig. 14. Wave function of a one-dimensional half-nucleon intruder state. Similar wave functions for the spherical WS potential used earlier are shown in Figs. 7 and 11.

The energies of these equations have been calculated as illustrated in Fig. 13. (A common value of $\delta = 0.1 \text{ fm}$ is used in all calculations.) We note that the energies are paired, in agreement with Eq. (22).

As also shown in Fig. 13, there is a clear level crossing behavior near $V_0 \simeq -1000 \text{ MeV}$. For potentials shallower than this value, the wave functions for the E_{n+} and E_{n-} states are dominated respectively by g and f . For potentials deeper, the energies of the E_{1+} and E_{1-} states are special, both being practically zero and independent of the potential depth, and their wave functions all have a special structure of either $f = -g$ or $f = g$ as illustrated in Fig. 14. Also for this potential range, the wave functions for the $(E_{n+}, n > 1)$ states are dominated by f as illustrated in Fig. 15. Similarly those for the $(E_{n-}, n > 1)$ states are dominated by g .

According to Eq. (20), the wave function (f, g) as a whole has a 'mixed parity' structure, in the sense that each of f and g is a function of definite parity but their parities are opposite. This is seen in Fig. 14 where g has positive parity while f has negative parity. Similar parity structure is also seen in Fig. 15. We note that Eq. (23) provides a convenient way for obtaining approximate wave functions near the walls and near the center of the potential. This has been helpful in explaining the shapes of

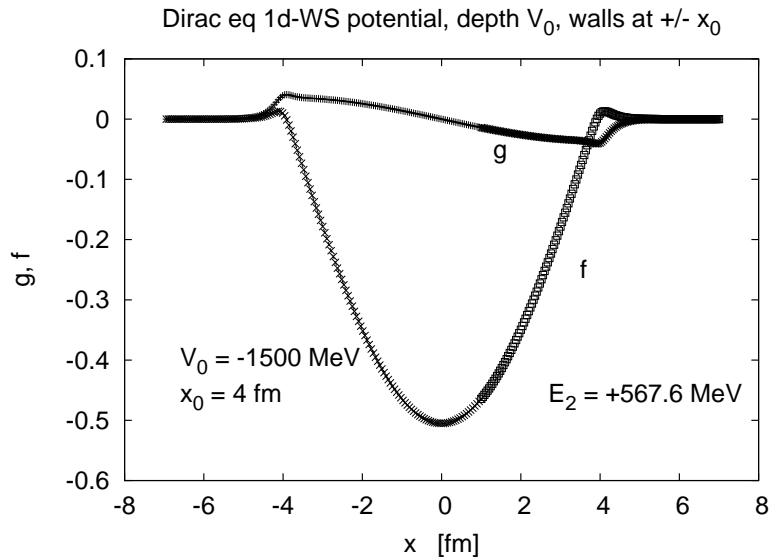


Fig. 15. Wave function of a one-dimensional positive-energy state with f dominance. Similar wave functions for the spherical WS potential used earlier are shown in Fig. 9

the wave functions of Eq.(20).

In short, the main features of the nucleon-anti-nucleon intruder states obtained from the spherical WS potential are well reproduced by the results from the one-dimensional WS potential.

References

1. G.E. Brown and T.T.S. Kuo, Nucl. Phys. **92**, 481 (1967).
2. T. T. S. Kuo and G. E. Brown, Nucl. Phys. **85**, 40 (1966).
3. G. E. Brown, *Unified Theory of Nuclear Models and Forces* (North-Holland, Amsterdam, 1971).
4. M. Hjorth-Jensen, T.T.S. Kuo and E. Osnes, Physics Report **261**, 126 (1995).
5. L. Coraggio, A. Covello, A. Gargano, N. Itaco and T. T. S. Kuo, Prog. Part. Nucl. Phys. **62**, 135 (2009).
6. G. E. Brown, T. T. S. Kuo, J. W. Holt and S. Lee, 'Nucleon-nucleon interactions and nuclear many-body problems', World Scientific Pub. Co. Singapore (2010).
7. H. Dong, T.T.S. Kuo and J.W. Holt, Nucl. Phys. **930**, 1 (2014).
8. T.T.S. Kuo, J.W. Holt and E. Osnes, Physica Scripta **91**, 033009 (2016).
9. T. H. Schucan and H. A. Weidenmueller, Ann. Phys. (N.Y.) **73**, 103 (1972); **76**, 483 (1973).

10. P.J. Ellis and E. Osnes, *Rev. Mod. Phys.* **49**, 777 (1977); C. M. Vincent and S. Pittel, *Phys. Lett.* **47B**, 327 (1973); P. A. Schaefer, *Ann. Phys.* **87**, 375 (1974).
11. G. E. Brown and M. Bolsteri, *Phys. Rev. Lett.* **3**, 377 (1959).
12. G. E. Brown and M. Rho, *Phys. Rev. Lett.* **66**, 2720 (1991).
13. G. E. Brown and M. Rho, *Phys. Rep.* **396**, 1 (2004) **253,252**(1991).
14. J. W. Holt, G.E. Brown, J.D. Holt and T.T.S. Kuo, *Nucl. Phys.* **A785**, 322 (2007).
15. J. W. Holt, G.E. Brown, T.T.S. Kuo, J.D. Holt and R. Machleidt, *Phys. Rev. Lett.* **100**, 062501 (2008).
16. L. W. Siu, J. W. Holt, T. T. S. Kuo and G. E. Brown, *Phys. Rev.* **C79**, 0540004 (2009).
17. H. Dong, T.T.S. Kuo and R. Machleidt, *Phys. Rev.* **C80**, 065803 (2009).
18. H. Dong, T.T.S. Kuo and R. Machleidt, *Phys. Rev. C* **83**, 054002 (2011).
19. H. Dong, T.T.S. Kuo, H. K. Lee, R. Macleidt and M. Rho, *Phys. Rev.* **C87**, 054332 (2013).
20. W. G. Paeng, T.T.S. Kuo, H. K. Lee and M. Rho, arXiv:1508.05210 (2015); *Phys. Rev. C*, to be published (2016).
21. P. E. Hodgson, 'The nucleon optical potential' (World Scientific Pub. Co. 1994).
22. Y. Nogami and F.M. Toyama, *Phys. Rev.* **C42**, 2449 (1990).
23. R. H. Landau, 'Quantum Mechanics II', John Wiley & Sons (1996).
24. R. R. Silbar and T. Goldman, *Eur. J. Phys.* **32**, 212 (2011).
25. 'Black Hole-Wikipedia', https://en.wikipedia.org/wiki/Black_hole.
26. B. Schutz, 'General Relativity', Cambridge Univ. Press (2009).
27. J. Antoniadis et al. *Science* **340**, 6131 (2013).
28. B. Mukhopadhyay and S. Chakrabarti, *Nucl. Phys.* **B852**, 629 (2000).
29. S. M. Carroll, 'Spacetime and Geometry', Addison and Wesley (2004).